Computers and Electronics in Agriculture 210 (2023) 107894

Contents lists available at ScienceDirect

Computers and Electronics in Agriculture

journal homepage: www.elsevier.com/locate/compag

# Development of improved flow analysis prototype method for measuring and understanding agricultural non-point source (NPS) nitrogen (N) and phosphorus (P) pollution

Linze Li [a,b,d], Liuzheng Ma [a,b], Hao Zhang [a,b], Junfeng Wu [a,b], Syed Muhammad Zaigham Abbas Naqvi [a,b], Zhengfeng Li [a], Wentao Wei [a,b,d], Muhammad Awais [a,b,c], Shixin Li [a], Babatunde Sunday Ewulo [e], Jiandong Hu [a,b,d,*]

[a] College of Mechanical and Electrical Engineering, Henan Agricultural University, Zhengzhou 450002, China
[b] Henan International Joint Laboratory of Laser Technology in Agriculture Sciences, China
[c] Department of Biochemistry and Molecular Biology, University of Sialkot, 51311 Sialkot, Punjab, Pakistan
[d] State Key Laboratory of Wheat and Maize Crop Science, Zhengzhou 45002, China
[e] Crop, Soil and Pest Management Department, Federal University of Technology, Akure, Nigeria

ARTICLE INFO

*Keywords:*
Chemical reaction chamber
Agricultural non-point source (NPS) pollution
Nitrogen and Phosphorus measurements
Improved flow analysis method
Pollution load evaluation

ABSTRACT

The loss of nitrogen (N) and phosphorous (P) through continuous surface runoff by rainfall after fertilizing and leaching into groundwater has become a critical issue that causes eutrophication of rivers, lakes, and even drinking water, resulting in agricultural non-point source (NPS) pollution of up to 50 % of pollution load. Traditionally, N and P were measured using the laboratory's flow injection analysis (FIA) method before evaluating the pollution load, which could meet urgent requirements in the fast response, prevention, and control of agricultural NPS pollution. Herein, we propose an improved flow analysis (perturbation dispersion) method by integrating chemical reaction chambers to measure nitrogen and phosphorus in water automatically and continuously. The as-fabricated system was validated with real samples from Qianjiang, Hubei Province. The experimental results drew a correlation coefficient of 0.91449 for ammonium nitrogen between the existing lab-based flow analysis method and the innovative (improved) flow analysis method. The correlation coefficients of 0.99828, 0.85129, and 0.99206 for nitrate nitrogen, ammonium nitrogen, and phosphorus were calculated from the measurement results. The detection limits of 0.55, 0.20, and 0.025 mg/L with relative standard deviations (RSD) of 0.8 %, 5.7 %, and 0.9 % were observed for $NH_4^+$–N, $NO_3^-$–N, and $PO_4^{3-}$ measurements, respectively. This work facilitates the online and continuous control of the NPS pollution load and timely expands the flow injection analysis (FIA) techniques for understanding the pollutants in water and farmland environments.

## 1. Introduction

Research and development of field measurement methods for evaluating agricultural non-point source (NPS) pollution in groundwater, typically for ammonium nitrogen ($NH_4^+$–N), nitrate nitrogen ($NO_3^-$–N), and phosphate ($PO_4^3$-), have attracted considerable attention during the last decade. Recommended doses of fertilizers applications are indispensable, yet, excessive applications of chemical fertilizers, including nitrogen and phosphorus fertilizers, still occur frequently (Rehman et al., 2022; Sun et al., 2022). The excess nitrogen (N) and phosphorus (P) in the form of $NH_4^+$, $NO_3^-$, and $PO_4^{3-}$ ions easily dissolve in water and are moved to another point or into the surrounding stream or water bodies.

The typical agricultural non-point source pollution of the water body by rainfall surface runoff of nutrients after fertilizing causes eutrophication that promotes harmful algae bloom reduces habitat for invertebrates and fish, fish-kills, and lowers fishery production, poor water quality, disruption of water transport and wide fluctuations in pH and dissolved oxygen (DO) or chronically low DO. Extensive fertilizer application also causes high nitrate in groundwater with attendant health problems, especially for an infant. (Fianko & Korankye, 2020; Timotewos & Daniel, 2020). A global map of soil pollution, including the

* Corresponding author at: College of Mechanical and Electrical Engineering, Henan Agricultural University, Zhengzhou 450002, China.
*E-mail address:* jdhu@henau.edu.cn (J. Hu).

https://doi.org/10.1016/j.compag.2023.107894
Received 6 October 2022; Received in revised form 21 April 2023; Accepted 27 April 2023

agricultural NPS, has been generated to prevent further corrosion by identifying sources, controlling polluter behavior, and reducing risks to public health and the environment (Hou & Ok, 2019). Although agricultural NPS pollution has multiple sources and the type and degree vary across regions, the Chinese government has taken several measures against soil pollution (Sills et al., 2018). The water pollution sources were contained in the once-a-decade census on pollution sources released in 2020 (Fig. 1). There are various water pollution sources in China; among them the animal and vegetable oil are majorly contributing. Among the agricultural NPS pollution the typical nitrogen and phosphorus from cropland are majorly contributing. Water pollution sources in the east-central of China, Henan province holds the major contribution by animal and vegetable oil, typical nitrogen and phosphorus and heavy metals. Whereas, the agricultural NPS pollution in Henan province holds a major contribution by typical nitrogen and phosphorus (CGTN, 2020).

The second decadal pollution census in China in December 2017 shows that agricultural non-point source pollution (typical nitrogen N and phosphorus P) remains the major source of groundwater pollution. Although, the pollution load has decreased from 57.2 % of the total nitrogen (TN) and 67.4 % of total phosphorus (TP) in 2010 to 36.79 % and 50.23 %, respectively, in 2017 in China (Hu et al., 2017). To evaluate pollutant load from agricultural NPS, measurement instruments and evaluation methods should be prepared in advance. Atomic absorption /emission spectroscopy and mass spectrometry (MS) are utilized in the laboratory to obtain accurate N and P results for evaluating agricultural NPS pollution (Pradela-Filho et al., 2020). However, they are costly, time-consuming, and inconvenient for detecting N and P on the field. Measurements of $NH_4^+$–N, $NO_3^-$–N, and Phosphate ($PO_4^{3-}$) are widely carried out with colorimetric analysis, such as UV–Vis spectrophotometry in the laboratory, N and P have been successfully measured using a multi-channel photoelectronic method. However, it is still operated manually (Xie et al., 2022).

One of the existing faster measurement systems has an NPK kit to measure the chemical properties of soil, but the results from the NPK kit need to be rectified before use (Yamin et al., 2020). Flow analysis methods are the most powerful techniques for fast measurement of $NH_4^+$–N, $NO_3^-$–N, and Phosphate ($PO_4^{3-}$) measurements (Taira et al., 2020). The typical flow analysis method involves dispersion, convection, and forced convection, which reduces reagent consumption by more than 90 % and minimizes operational errors (Ferguson & Meyerhoff, 2017; Zagatto & Rocha, 2021). The existing flow analysis method shows that nitrogen and phosphorus measurement results have a good correlation coefficient without significant differences in comparison with conventional lab-based methods [Table 1]. The improved flow analysis can measure the concentrations of $NH_4^+$–N, $NO_3^-$–N, and Phosphate ($PO_4^{3-}$) with lowest detection limits as compared to the typical flow analysis method (Diamond et al., 2017; Jones et al., 2017). This measurement system consists of a microsyringe pump, two peristaltic pumps, one multi-channel solenoid valve, two holding loop rings, a specified chemical reaction chamber, and a modular photoelectric detection unit. Specifically, both the chemical reaction chamber and the modular photoelectric detection unit were utilized to realize a steady-state measurement of N and P in a flow analysis mode instead of transient measurement.

The purpose of this novel study is to carry out an automatic measurement of N and P using an improved flow analysis method. The accuracy and precision of the improved flow system were successfully compared with the conventional method for the actual sample. Nitrate-nitrogen, ammonia nitrogen, and phosphorus were determined continuously by connecting a novel chemical reaction chamber.

## 2. Materials and methods

Sample materials were collected from cropland in Luohe (Henan Province) and Qianjiang and Yichang (Hubei Province) to validate and compare improved flow analysis accuracy with a lab-based method. The sample solutions for measuring $NH4^+$–N, $NO3^-$–N, and $PO4^{3-}$ were filtered through a 0.45 μm microporous membrane. The UV–Vis spectral data were recorded on a spectrometer at room temperature.

### 2.1. The improved flow analysis system structure and setup

An improved flow analysis system for the measurements of N and P

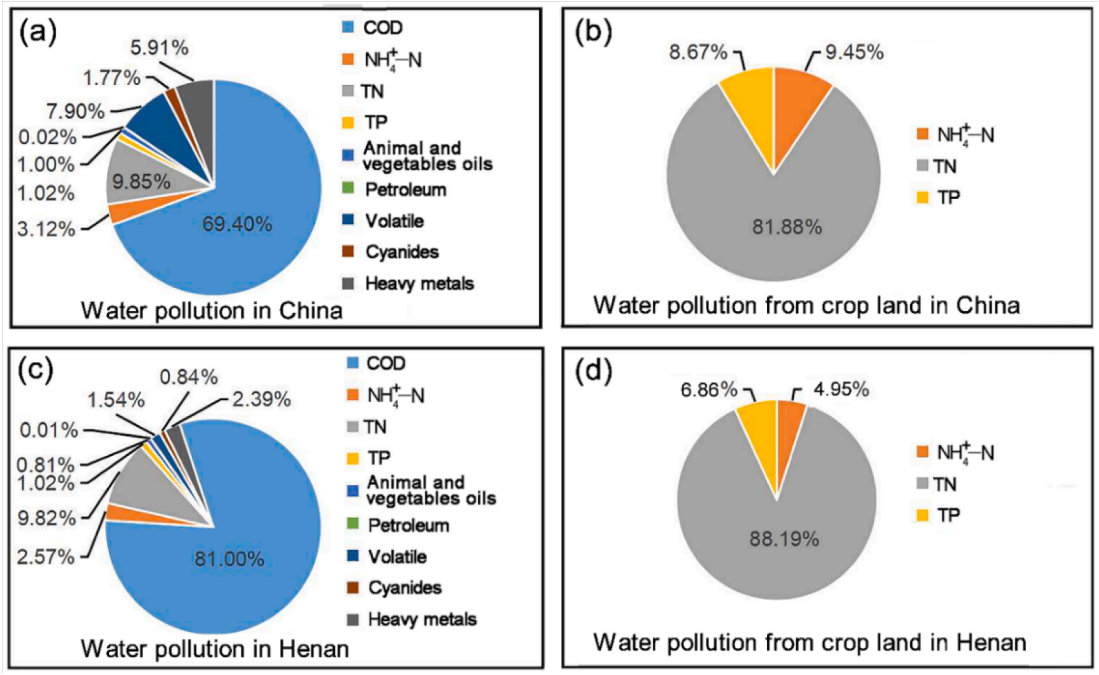


**Fig. 1.** The year 2020 China's Environmental Protection Second National Census on Pollution Sources. (a) Water Pollution Sources in China. (b) Agricultural Non-Point Source Pollution (typical nitrogen and phosphorus from cropland) in China. (c) Water Pollution Sources in the East-Central of China, Henan Province. (d) Agricultural Non-Point Source Pollution in Henan Province (CGTN, 2020).

**Table 1**
Reported flow analysis methods for measuring Nitrogen and Phosphorus from soil samples.

| Methods | Reagents | Dynamic Range | Measurement time (determinations $h^{-1}$) | LOD | References |
|---|---|---|---|---|---|
| FA | Sulfuric acid, ammonium heptamolybdate tetrahydrate, potassium chloride, potassium dihydrogen phosphate, potassium nitrate, Cu(II) standard solution | 100 ppm | – | 6 μM | (Talarico et al., 2015) |
| FIA | potassium nitrate, ammonium chloride, and urea, Glycine and L-glutamic acid, adenosine 5′-monophosphate monohydrate, potassium dihydrogen phosphate, 2-aminoethylphosphonic acid, O-phosphorylethanolamine, sodium tripolyphosphate | 300 μmol $L^{-1}$,25 μmol $L^{-1}$ | 5 | 0.8 μmol $L^{-1}$,0.2 μmol $L^{-1}$ | (Lin et al., 2018) |
| SIA | potassium dihydrogen phosphate, ammonium molybdate tetrahydrate, potassium antimonyl (III) tartrate, L-ascorbic acid | 0.1–6 mg P $L^{-1}$ | 30 | 0.1 mg $L^{-1}$ | (Khongpet et al., 2018) |
| MPFS | $CaCl_2$, $KH_2PO_4$, bismuth as $(BiO)_2CO_3$, ammonium heptamolybdate as $(NH_4)_6Mo_7O_{24}$, sulfuric acid solution, ascorbic acid ($C_6H_8O_6$) solution, $HNO_3$, stannous chloride as $SnCl_2$ | 51 μg $L^{-1}$ | 87 | 17 μg $L^{-1}$ | (Machado et al., 2017) |

FA = Flow analysis, FIA = Flow injection analysis, SIA = Sequential injection analysis, MPFS = multi-pumping flow system, LOD = Limit of detection.

was constructed (Fig. 2). This measurement system consists of a microsyringe pump, two peristaltic pumps, one multi-channel solenoid valve, two holding loop rings, a specified chemical reaction chamber, and a modular photoelectric detection unit. Specifically, the chemical reaction chamber and the modular photoelectric detection unit were utilized to realize a steady-state measurement of N and P in a flow analysis mode instead of transient measurement. First, the measured sample solutions and the required reagents were separately injected into the chemical reaction chamber by the microsyringe pump associated with the multi-channel solenoid valve, resulting in a diffused chemical reaction in the reaction chamber. Then a peristaltic pump repeatedly perturbs the reactant in the chemical reaction chamber to generate a turbulence flow to improve the chemical reaction efficiency. Finally, the reactant flows through the modular photoelectric detection unit custom-tailored for N and P measurements (Fig. 2b).

The measurement process is specified as follows: the samples and reagents were precisely quantitated by a microsyringe pump in conjunction with a sample loop and then injected into the chemical reaction chamber sequentially. After that, a perturbed reaction in the chemical reaction chamber was repeatedly arranged with a peristaltic pump, resulting in turbulence to improve the chemical reaction. Once the chemical reaction reached equilibrium, the reactant was guided to flow through a modular photoelectric detection unit to record the absorption spectra. This improved flow analysis method exhibited good absorption spectral performances and low detection limits for N and P measurements.

The chemical reaction chamber consisted of a top cover with a spray head, a mixing chamber, and a bottom end cover. The mixing chamber was made of quartz glass, and the inner wall was coated with a hydrophobic material to synthesize the residual liquid on the inner wall into droplets, which fell down onto the bottom cover on account of their weight. The flow speed of the reactant was controlled and programmed by the peristaltic pump so that the highest point of liquid sprayed in the chemical reaction chamber reached 2/3 of the height of the chamber. The peristaltic pump first draws the reactant into the mixing chamber, and the reactant gets induced into a holding loop. The peristaltic pump reversely pumps the reactant back into the mixing chamber and air into the mixing chamber. This disturbs the reactant and accelerates the chemical reaction process. Recirculation, eddies, and apparent randomness with the aid of the peristaltic pump produced turbulence in the chemical reaction chamber. In turbulent flow, the speed of the reactant at a point undergoes changes in magnitude and direction by the peristaltic pump controlled by the embedded programming software. The root-mean-square (RMS) quantities characterize the concentration at a particular point in both time and space.

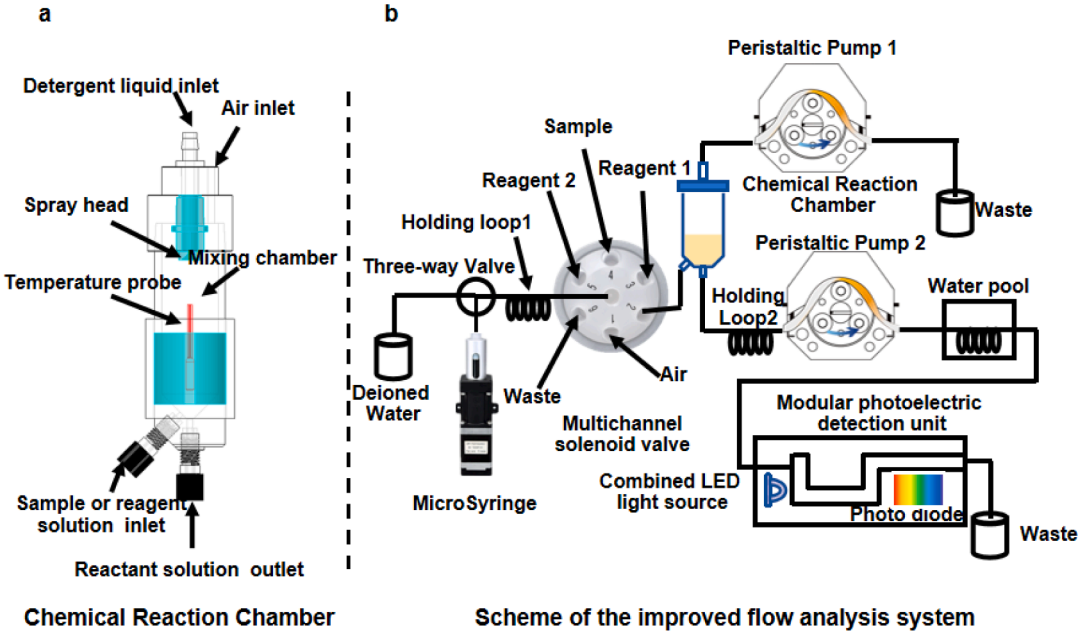


**Fig. 2.** Structure of Improved Flow Analysis System. (a) Structure of Chemical Reaction Chamber. (b) Scheme of the Improved Flow Analysis System.

### 2.2. Modular absorption spectra measurement system with a microfluidic tube

The modular photoelectric detection unit is specified and designed for N and P measurements. A combined LED light source module, a highly sensitive photodiode, a microfluidic tube with optical path lengths of 10 mm, 20 mm, and 30 mm, optionally, and two PIC microcontroller-based circuit boards were incorporated into this configuration (Fig. 3b). One most promising optical path length can be confirmed according to the lowest concentration of the detected samples. The chemical reaction chamber and pipelines are cleaned programmatically in this absorption spectra measurement system by controlling peristaltic pumps. Therefore, the absorption spectra can realize the continuous measurement without replacing the pipelines.

The flow chart of the modular absorption spectra measurement system (Fig. 3a), circuit schematics of the optoelectric acquisition, and the driving current of the combined LED light source (Fig. 3c and d) are shown in Fig. 3.

The circuit mainly comprises GS8552 (U101), a zero-drift CMOS operational amplifier with very low offset voltage, and CS1233 (U102), a 24-bit analog-to-digital converter. J101 and J102 were connected to the power supply and the photodiode sensor. The wavelengths of the combined LED light source were 405 nm, 440 nm, 515 nm, 540 nm, 640 nm, 880 nm, and 660 nm, optionally according to the measurement requirement. A variable resistor (VR), AD8400 (U201 in Fig. 3d), is 256-position digitally controlled by the microcontroller through a Serial Peripheral Interface (SPI). A zero-drift CMOS (Complementary Metal-Oxide-Semiconductor) operational amplifier, GS8562 (U202), was used to drive the p-channel MOS transistor (Q204) to ensure constant output current of the combined LED light source, working at different wavelengths optionally. In this modular photoelectric detection unit, two PIC microcontroller circuit boards are connected to the main circuit board via an RS-485 cable (Fig. 3b).

### 2.3. Design of improved prototype flow analysis system

A circuit board using a PIC microcontroller (PIC32MZ0512, U501) (Fig. 4b) was developed to provide the driving current for the combined LED light sources. The wavelengths of light source for the measurements of nitrate nitrogen, ammonium nitrogen, and phosphorus were controlled programmatically, while the microfluidic tube was embedded in the middle of this module. Another PIC microcontroller circuit board was designed to acquire the photoelectric signals from the photodiodes. Both PIC microcontroller circuit boards were placed on the two ends of the microfluidic tube and connected to the main circuit board via RS-485 cable (main board).

The concentrations of nitrogen and phosphorus vary greatly in time and space. Therefore, the lengths of the optical path lengths of 10 mm, 20 mm, and 30 mm were optioned to meet measurement accuracy requirements due to the absorbance proportional to optical length, $A(\lambda) = \alpha \times C \times L$, where $A$ is the absorbance for a given wavelength, α is the molar absorptivity, $L$ is the distance that the light travels through the sample solution, and $C$ is the concentration of the absorbing species. The PIC microcontroller (U501) manages the microsyringe pump, the peristaltic pump, pinch valves, and the multi-channel solenoid valve through the Modbus RTU (Remote terminal unit) protocol programmatically. In RTU, the master RS-485 ports can be configured in 8 N1 mode with a baud rate of 9600 bps (8 data bits, 1 start bit, no parity, and 1 stop bit. However, the slave RS-485 ports were configured as 8e1 mode with a baud rate of 9600 bps (8 data bits, even parity bit, 1 start bit, and 1 stop bit).

### 2.4. Theoretical simulation of absorption wavelengths of detected ions in water environment and UV–Vis spectrophotometry measurement experiment

The density functional of M06-2X with good performance on main-group elements was used to optimize the structures of ions of interest combined with the basis set of 6-311+G (2d,p). Frequency calculations were made to ensure the local minimum of potential surface. The SMD (Solvation Model Based on Density) implicit solvation model of water was used to render the aqueous situation (Marenich et al., 2009).

The computational UV–Vis spectra were calculated at the same level of theory by time-dependent density functional theory (TDDFT) (Liu et al., 2020), a compromised performance on the excitation energy calculation. Gaussian 16 program was applied in all the above calculations (Zhao and Truhlar, 2007). In the computable UV–Vis spectra, the obvious adsorption band at 203 nm was assigned to $NO_3^-$ (Supplementary Fig. S1a); this is close to the adsorption band of $NO_3^-$ in the standard experimental UV–Vis spectra. In this manner, the band near 205 nm in UV–vis spectra of soil leaching solution can be used to reflect the content of $NO_3^-$–N, as other interfering ions were excluded. Thus, the standard curves for the UV–Vis spectra method can be obtained (Supplementary Fig. S1b). The *ab initio* calculation accurately determines the maximum adsorption for plotting a standard curve based on the UV–Vis spectra.

Before determining the wavelengths for this measurement, the detected sample solutions were arranged to obtain the absorption wavelengths in the range of 400 nm-1100 nm of nitrate nitrogen, ammonium nitrogen, and phosphorus, respectively, with the lab-based UV–Vis spectrophotometer, suggesting that most molecules remained in the form of corresponding ions. The sensitivity of the effective phosphorus sample tested at the absorption peak of 880 nm (the effective phosphorus-molybdenum blue colorimetric method) was calculated.

### 2.5. Establishment of the calibration curve for N and P measurements

In evaluating agricultural NPS pollution load, the measurements of nitrogen and phosphorus were relatively easy in the laboratory; running measurements on the field automatically presented some challenges. The measurement of nitrate nitrogen ($NO_3$–N) (known to be directly available to plants) was used to provide indicators of short-term nitrogen availability and evaluate its loss. Known concentrations of ammonium nitrogen solution (0 mg/l, 1.0 mg/l, 2.0 mg/l, 3.0 mg/l, and 4.0 mg/l) nitrate nitrogen (0 mg/l, 0.5 mg/l, 1.0 mg/l, 1.5 mg/l, 2.0 mg/l, and 2.5 mg/l) and phosphorus concentrations (0 mg/l, 0.5 mg/l, 1.0 mg/l, 2.0 mg/l, and 3.0 mg/l) were arranged to establish their absorbance curve (Fig. 5).

### 2.6. Assessment of the accuracy and precision of the measurement system for actual samples

Temperature and optical path length were set prior to running the improved flow analysis system. Ten (10) samples were collected from Luohe (Henan Province) and Qianjiang and Yichang (Hubei Province). In the experiment, 37℃ temperature was set through a proportional integral derivative (PID) controller, and the optical path length of 20 mm was chosen. The 10 samples were divided into two equal parts. The improved flow analysis system measured the first part to determine the concentrations of the $NH_4^+$–N, $NO_3^-$–N, and phosphorus. The other part was measured by the conventional method with a commercialized UV–Vis spectrophotometer, where the nitrate nitrogen was determined using both wavelengths of 220 nm and 275 nm, to reduce the interference in the measured sample solution.

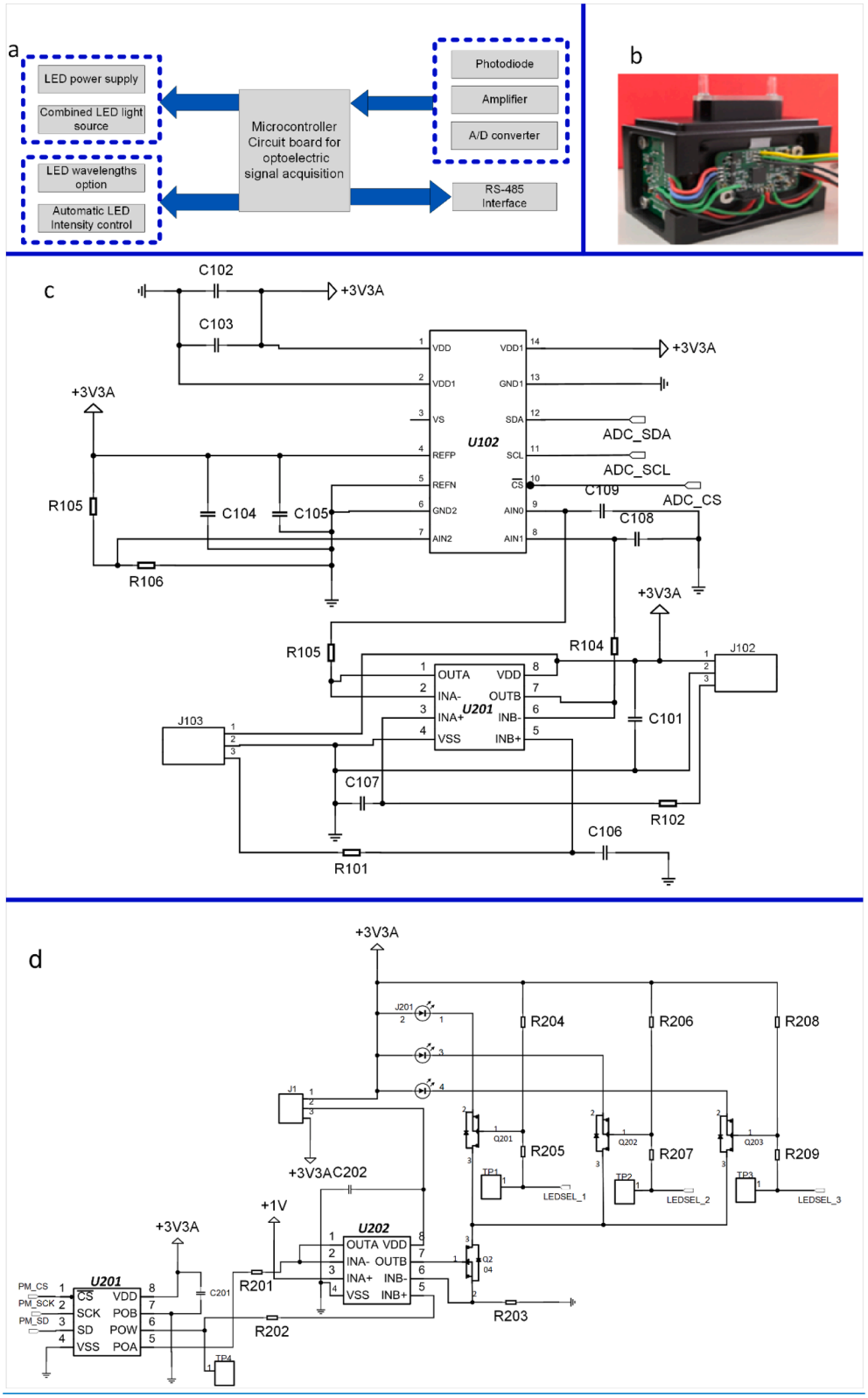


**Fig. 3.** Modular Temperature Regulated Photoelectric Detection Unit (including a temperature controller, a microfluidic tube, and a combined LED light source board). (a) Design a Flow Chart of the Modular Absorption Spectra Measurement System. (b) Prototype of the Photoelectric Detection Unit. (c) Schematics of the Photoelectric Acquisition Circuit. (d) Combined LED Light Source Driving Circuit.

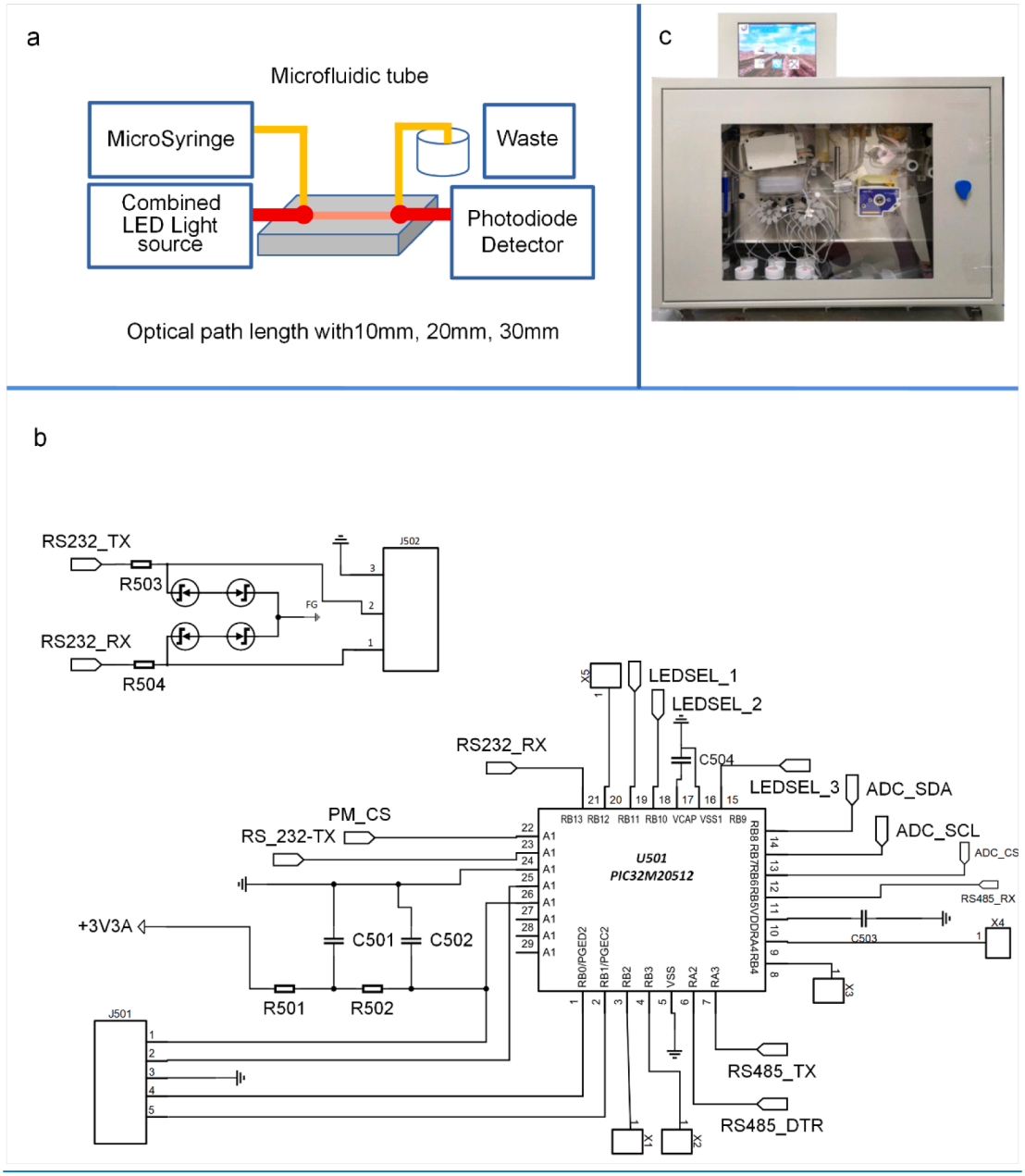


**Fig. 4.** Measurement principle and prototype of the improved flow analysis system. (a) scheme of the flow analysis method. (b) design of the circuit board using a PIC microcontroller (PIC32MZ0512, U501). (c) prototype of the improved flow analysis system.

## 3. Results and discussion

The relationships between known concentrations of nitrate nitrogen and its absorbance values results (Fig. 5b) were established from the absorption peaks at 550 nm, 660 nm, and 880 nm, respectively. They were consistent with the typical absorption wavelengths of nitrate nitrogen, ammonium nitrogen, and phosphorus.

The calibration curves for N and P measurements showed good linear relationships between known concentrations of ammonium nitrogen, nitrate nitrogen, and phosphorus and their absorbance values with the correlation coefficient of 0.99793, 0.99779, and 0.99997, respectively (Fig. 5a–c). The detection limit of $NH_4^+$–N, $NO_3$–N, and $PO_4^{3-}$ were 0.55, 0.20, and 0.025 mg/L, respectively (Fig. 5d).

The correlations between the improved flow analysis method and conventional UV–Vis spectrophotometer measurements are shown in Fig. 6; a correlation coefficient of 0.91499 was obtained between the measured values of ammonium nitrogen using this improved flow analysis system under the combined extractant of sodium sulfate and sodium bicarbonate and the conventional measured values. Correlation coefficients of 0.99828, 0.85129, and 0.99206 under the calcium chloride extractant were calculated (Fig. 6b–d). Therefore, the improved flow analysis method showed a good correlation with conventional methods and can meet the requirement for measuring $NH_4^+$–N, $NO_3^-$–N, and Phosphate ($PO_4^{3-}$) automatically.

In order to compare nitrogen (N) measurement using an AA3 type flow injection analyzer, the continuous-Flow AutoAnalyzer III (AA3) for measuring $NH_4^+$–N, $NO_3^-$–N was applied in this experiment. The standard concentrations of 0.25, 0.50, 1.00, and 2.00 ppm of ammonium nitrogen solutions and the standard nitrate nitrogen of 0.50, 1.00, 2.00, and 4.00 ppm were supported by Beijing Coast Hongmeng standard substance technology Co., Ltd. The measurement results (n = 5) are shown in Table 2. The maximum relative error of 7.8 % was calculated from the

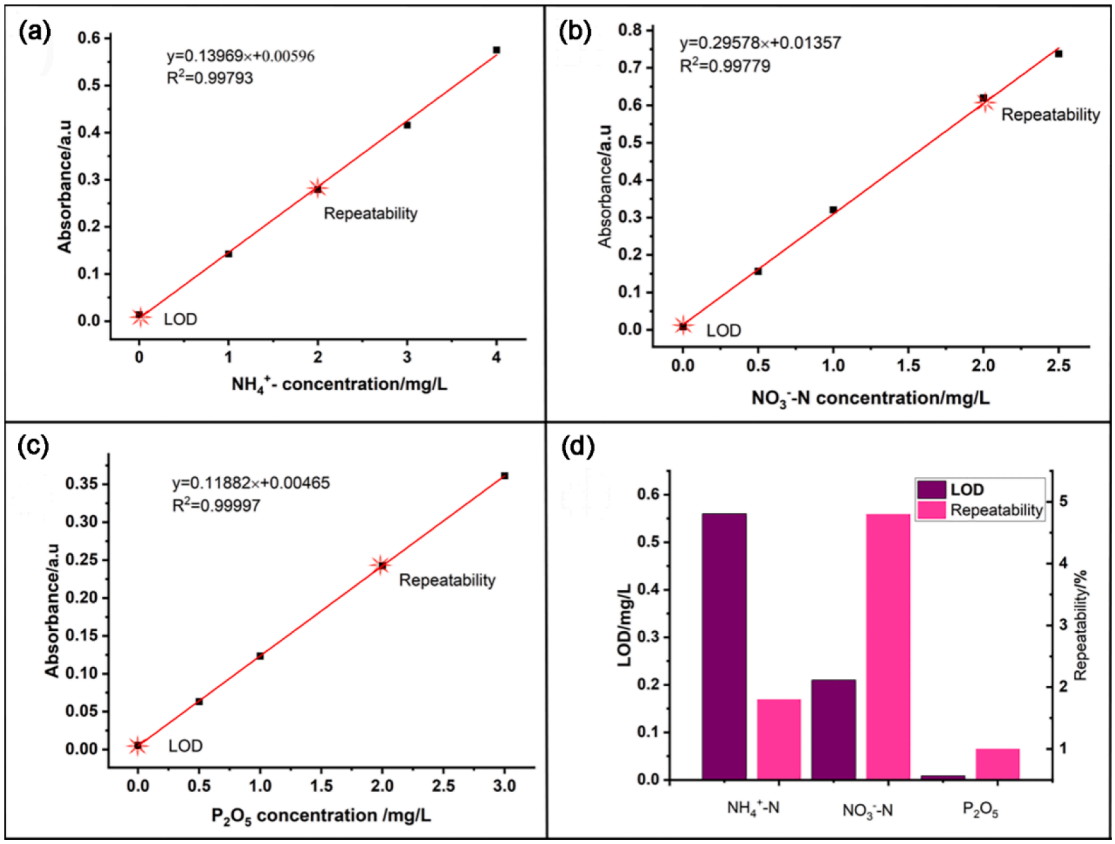


**Fig. 5.** Absorbance measurements of the known concentrations of $NH_4^+$–N, $NO_3^-$–Nand $PO_4^{3-}$. (a) Relationships between known concentrations of ammonium nitrogen and its absorbance values. (b) Relationships between known concentrations of nitrate nitrogen and its absorbance values. (c) Relationships between known concentrations of phosphorus and its absorbance values. (d) Detection limit graph of $NH_4^+$–N, $NO_3^-$–N, and $PO_4^{3-}$.

AA3 flow injection analyzer in the measurement of ammonium nitrogen, and the maximum relative error of 3.6 % in nitrate nitrogen measurement. However, in the measurements of the ammonium nitrogen and the nitrate nitrogen, the maximum relative error of 6.0 % was obtained from the improved flow analysis system. It shows that both methods are comparable, but the cost of the improved flow analysis method is greatly reduced.

In the improved flow analysis system, only one microfluidic tube was used for N and P measurements to eliminate errors caused by inconsistent channels in the multi-channel measurement system. The absorbance compensation algorithm was ignored. Different soil extraction systems are internationally applied in the measurement of N and P; flexible parameters can be set according to measurement standards and regulations prior to actual sample measurement. Computational UV–Vis spectra were successfully calculated from optimized structures of ions of interest and adsorption band at 203 nm assigned to $NO_3^-$, thereby facilitating standard curves for the UV–Vis spectra.

Absorbance curves were also successfully established for ammonium nitrogen, and phosphorus concentrations with good linear relationships between known concentrations and absorbance values. Absorption peaks at 550 nm, 660 nm, and 880 nm were obtained, respectively, which are consistent with the typical absorption wavelengths of nitrate nitrogen, ammonium nitrogen, and phosphorus. The improved flow analysis method, showed a good correlation with conventional methods and can automatically meet the requirement for measuring $NH_4^+$–N, $NO_3^-$–N, and $PO_4^{3-}$ automatically. Results indicated that the improved method is better than the traditional method by analyzing the correlations between the improved flow analysis method and the conventional method. Therefore, the comparative analysis indicates the improved flow analysis system's significantly comparable and reproducible results of improved flow analysis system.

## 4. Conclusion

The accuracy and precision of the improved flow system were successfully compared with the conventional method for the actual sample. The improved flow analysis method showed a good correlation (i.e., accuracy) with conventional methods ($R^2$ = 0.99828, 0.85129, and 0.99206 for ammonium nitrogen, nitrate nitrogen and phosphate, respectively). The performance characteristics of the system for the determination of $NH_4^+$–N, $NO_3^-$–N, and Phosphate ($PO_4^{3-}$) were successfully verified. A maximum relative deviation of 6.00 % was achieved in comparison with the continuous-Flow AutoAnalyzer III (AA3) for the measurements of $NH_4^+$–N and $NO_3^-$–N compared with the conventional UV–Vis spectrophotometric method. Correlation coefficient of 0.91449 was calculated for $NH_4^+$–N measurement using the extractant of sodium sulfate and sodium bicarbonate. The correlation coefficients of 0.99828, 0.85129, and 0.99206 were calculated using the extractant of calcium chloride for $NH_4^+$–N, $NO_3^-$–N, and Phosphate ($PO_4^{3-}$), respectively.

The experimental result shows that improved flow analysis can measure the concentrations of $NH_4^+$–N, $NO_3^-$–N, and Phosphate ($PO_4^{3-}$) with low detection limits of 0.55, 0.20, and 0.025 mg/L, respectively. Future work is required to understand the principle of the improved flow analysis method with perturbation-diffusion kinetics to improve the accuracy of spectra absorption. Also, the novel measurement system needs further investigation for monitoring more compounds to evaluate the agricultural NPS pollution load in the field remotely and automatically.

## Funding

This research was financially supported by the National Natural Science Foundation of China [No. 32071890], the Special Key R&D

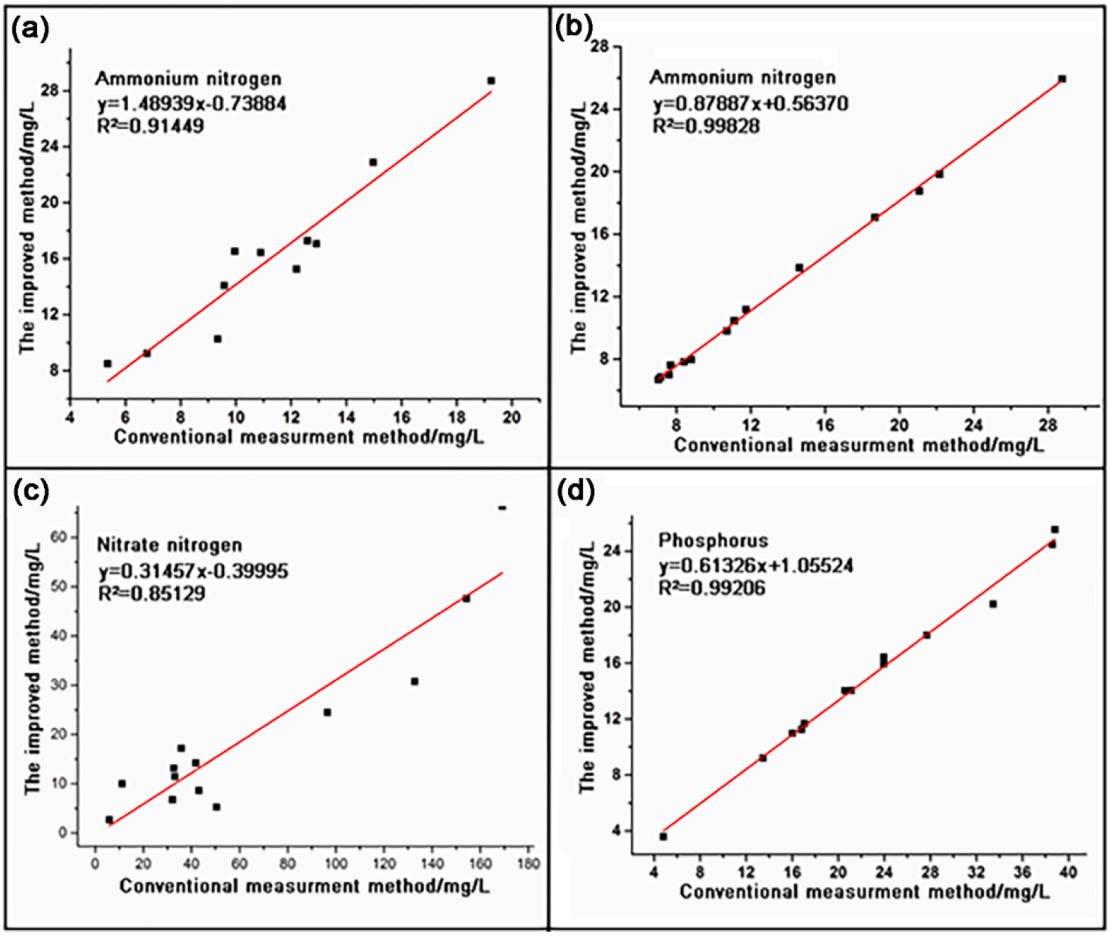


**Fig. 6.** Verification of available nitrogen and phosphorus samples measured by the integrated reaction flow analysis. (a) Indophenol blue method for ammonium nitrogen; (b) Nessler's reagent method for ammonium nitrogen; (c) Diazotization coupling reaction method for nitrate; (d) Molybdenum blue method for available phosphorus.

**Table 2**
Comparison between standard ammonium nitrogen analyzer and continuous -Flow Auto-Analyzer III (AA3) for the determination of $NH_4^+$–N and $NO_3^-$–N.

| Standard ammonium-nitrogen ($NH_4^+$–N) ( ppm ) | The continuous-Flow Auto-Analyzer III (AA3) ( ppm ) | Relative errors% | This method ( ppm ) | Relative errors % |
|---|---|---|---|---|
| 0.25 | 0.123 | – | 0.25 | – |
| 0.50 | 0.473 | 5.40 | 0.48 | 4.00 |
| 1.00 | 0.942 | 5.80 | 0.94 | 6.00 |
| 2.00 | 1.844 | 7.80 | 1.94 | 3.00 |
| Standard nitrate-nitrogen ($NO_3^-$–N) ( ppm ) | | | | |
| 0.50 | 0.518 | 3.60 | 0.53 | 6.00 |
| 1.00 | 0.976 | 2.40 | 0.94 | 6.00 |
| 2.00 | 1.967 | 1.65 | 1.92 | 4.00 |
| 4.00 | 3.936 | 1.6 | 3.91 | 2.25 |

Projects of Henan Province [No. 221111320700], the Henan Center for Outstanding Overseas Scientists [No. GZS2021007] and the National Key Technologies R & D Program of China during the 14th Five-Year Plan period [2021YFD1700904).

## CRediT authorship contribution statement

**Linze Li:** Formal analysis, Writing – original draft. **Liuzheng Ma:** Conceptualization, Methodology. **Hao Zhang:** Project administration. **Junfeng Wu:** Visualization, Resources. **Syed Muhammad Zaigham Abbas Naqvi:** Writing – review & editing. **Zhengfeng Li:** Validation. **Wentao Wei:** Data curation. **Muhammad Awais:** Investigation. **Shixin Li:** Resources. **Babatunde Sunday Ewulo:** Methodology. **Jiandong Hu:** Funding acquisition, Supervision.

## Declaration of Competing Interest

The authors declare that they have no known competing financial interests or personal relationships that could have appeared to influence the work reported in this paper.

## Data availability

Data will be made available on request.

## Acknowledgments

The authors are thankful to Henan Agriculture University for providing the research facilities.

## References

CGTN, 2020. China's Environmental Protection.
Diamond, D.H., Heyns, P.S., Oberholster, A.J., 2017. Accuracy evaluation of sub-pixel structural vibration measurements through optical flow analysis of a video sequence. Measurement 95, 166–172.

Ferguson, S.A., Meyerhoff, M.E., 2017. Manual and flow-injection detection/quantification of polyquaterniums via fully reversible polyion-sensitive polymeric membrane-based ion-selective electrodes. ACS Sens. 2, 1505–1511.
Fianko, J.R., Korankye, M.B., 2020. Quality characteristics of water used for irrigation in urban and peri-urban agriculture in Greater Accra Region of Ghana: Health and environmental risk. West African J. Appl. Ecol. 28, 131–143.
Hou, D., Ok, Y.S., 2019. Soil pollution – speed up global mapping. Nature 455.
Hu, Q., Zhao, X., Yang, X.J., 2017. China's decadal pollution census. Nature 543, 491.
Jones, T.R., White, J.W.C., Steig, E.J., Vaughn, B.H., Morris, V., Gkinis, V., Markle, B.R., Schoenemann, S.W., 2017. Improved methodologies for continuous-flow analysis of stable water isotopes in ice cores. Atmos. Meas. Tech. 10, 617–632.
Khongpet, W., Pencharee, S., Puangpila, C., Kradtap Hartwell, S., Lapanantnoppakhun, S., Jakmunee, J., 2018. Exploiting an automated microfluidic hydrodynamic sequential injection system for determination of phosphate. Talanta 177, 77–85.
Lin, K., Pei, J., Li, P., Ma, J., Li, Q., Yuan, D., 2018. Simultaneous determination of total dissolved nitrogen and total dissolved phosphorus in natural waters with an on-line UV and thermal digestion. Talanta 185, 419–426.
Liu, D., Shi, L., Gao, S.-H., Wu, Y.-H., Li, G.-Y., Zhou, C.-H., 2020. Twisted intramolecular charge transfer: A time-dependent density functional theory study on the sensing mechanism of a Schiff base sensor for fluoride. Chem. Phys. Lett. 738, 136894.
Machado, J., Melchert, W.R., Zagatto, E.A.G., Kamogawa, M.Y., 2017. A multi-pumping flow system with pulsed fluidization to evaluate soil capacity for phosphate adsorption. J. Brazilian Chem. Soc. 28, 1149–1157.
Marenich, A.V., Cramer, C.J., Truhlar, D.G., 2009. Universal solvation model based on solute electron density and on a continuum model of the solvent defined by the bulk dielectric constant and atomic surface tensions. J. Phys. Chem. B 113, 6378–6396.
Pradela-Filho, L.A., Noviana, E., Araújo, D.A.G., Takeuchi, R.M., Santos, A.L., Henry, C. S., 2020. Rapid analysis in continuous-flow electrochemical paper-based analytical devices. ACS Sensors 5, 274–281.
Rehman, A., Saba, T., Kashif, M., Fati, S.M., Bahaj, S.A., Chaudhry, H., 2022. A revisit of internet of things technologies for monitoring and control strategies in smart agriculture. Agronomy 12, 127.
Sills, J., Zhou, Y., Liu, Y., 2018. China's fight against soil pollution. Science 362, 298.
Sun, X., Ritzema, H., Huang, X., Bai, X., Hellegers, P., 2022. Assessment of farmers' water and fertilizer practices and perceptions in the North China Plain. Irrig. Drain. 1–17.
Taira, K., Hemati, M.S., Brunton, S.L., Sun, Y., Duraisamy, K., Bagheri, S., Dawson, S.T. M., Yeh, C.-A., 2020. Modal analysis of fluid flows: Applications and outlook. AIAA J. 58, 998–1022.
Talarico, D., Cinti, S., Arduini, F., Amine, A., Moscone, D., Palleschi, G., 2015. Phosphate detection through a cost-effective carbon black nanoparticle-modified screen-printed electrode embedded in a continuous flow system. Environ. Sci. Tech. 49, 7934–7939.
Timotewos, M., Daniel, R., 2020. Kulfo river stream impact on the sustainability of aquatic life in Chamo Lake at Arba Minch. J. Water Resources Ocean Sci. 9, 48–55.
Xie, X., Xu, L., Li, X., Li, D., 2022. Time-division-multiplexed online gauss-newton-based multi-echo decomposition method for real-time in-situ laser ranging. IEEE Sens. J. 22, 4152–4163.
Yamin, M., Bin Wan Ismail, W.I., Bin Mohd Kassim, M.S., Abd Aziz, S.B., Akbar, F.N., Shamshiri, R.R., Ibrahim, M., Mahns, B., 2020. Modification of colorimetric method based digital soil test kit for determination of macronutrients in oil palm plantation. Int. J. Agric. Biol. Eng. 13, 188–197.
Zagatto, E.A.G., Rocha, F.R.P., 2021. Large-scale flow analysis: From repetitive assays to expert analyzers. Talanta 233, 122479.
Zhao, Y., Truhlar, D.G., 2007. MN-GFM: Minnesota Gaussian functional module. University of Minnesota, Minneapolis, p. version 4..